

# Bioinspired Inchworm- and Earthworm-like Soft Robots with Intrinsic Strain Sensing

Prakash Karipoth, Adamos Christou, Abhilash Pullanchiyodan, and Ravinder Dahiya\*

Stimulus-responsive soft structures, with biological organs like intrinsic sensing, are needed to enable controlled movements and hence bring the transformative advances in soft robotics. Herein, bioinspired inchworm- and earthworm-like soft structures with intrinsic strain sensing achieved by seamless embedding of a graphite-paste-based sensor material are presented. The developed strain sensor exhibits a record stretchability (900%) and sensitivity (of  $10^3$  up to  $\approx 200$  and of the order of  $10^5$  at around 700% linear strain). With tiny permanent magnets incorporated at the ends of these soft structures, the sensory-feedback-based controlled movements of magnetically driven inchworm- and earthworm-like soft robots are also demonstrated. The presented results potentially boost the prospects of self-sensing in soft robots and advance the field toward cognitive soft robotics.

As a result, most of the biomimetic soft robots reported so far have imitated simple movement patterns of biological organisms.<sup>[7,8]</sup> On the contrary, the complex movements in biological organisms are coordinated by proprioceptive sensory receptors and the nervous system. Such movements in soft robotics can be attained with sensors such as thermally/electrothermally driven bimorph soft actuators<sup>[6e]</sup> and triboelectric nanogenerator-based sensors.<sup>[6f]</sup>

Unlike soft robots, the conventional rigid robots do not involve high degree of stretchability, or deformation, except at locations such as joints. Hence, stiff sensors were sufficient for closed-loop control in rigid-bodied robots.<sup>[9]</sup> However, such

## 1. Introduction

The way biological organisms use proprioception to perceive their position in space and to adapt to uncertain environments by changing postures has intrigued and inspired scientists to develop biomimetic engineered systems. These include soft robots with soft, stretchable, and deformable materials enabling infinite degrees of freedom.<sup>[1]</sup> For example, by imitating the simple locomotion patterns of worms<sup>[2,3]</sup> belonging to the phylum of arthropods<sup>[4]</sup> and annelids,<sup>[5]</sup> researchers have demonstrated the potential of using robots in constrained environments such as moving through a narrow hole. Such imitations of movements raise the hope that with further advances it will be possible to enable autonomous soft robots to conduct complex tasks such as grasping and controlled manipulation of objects. However, the literature on soft robotics shows that real-time sensory feedback, which is critical for such controlled locomotion or tasks, is generally missing.<sup>[6a–d]</sup>

approaches in soft robotics are challenging due to difficulties related to integration or embedding of stiff devices in the flexible and deformable structures. The stiff devices also constrain the movements or bendability and due to the huge mismatch in mechanical properties of stiff sensors and soft robotic body, the overall system is prone to failure.<sup>[6c,d,10]</sup> Further, the dynamics of soft robots are usually more complex due to the nature and distribution of driving stimulus and the nonuniform mechanical properties of composite materials and as a result it is difficult to sense all conformations under external stimulus.<sup>[6c]</sup> The hysteresis and nonlinear behavior of the commonly used soft elastomeric materials also make it difficult to use stiff sensors to control the movements.<sup>[11]</sup> The above challenges explain why almost all the soft robotic manipulation and control works so far have been demonstrated with no or little sensory feedback. They have been conducted either by preprogrammed stimulus variations or by instantaneous manual adjustments.<sup>[12]</sup> The hyperelastic complex deformation of the soft objects makes it difficult to develop accurate models. Also, most of the current models consider sensing and actuation as separate entities.<sup>[13]</sup> As a result, the demonstrations under laboratory conditions may not yield desired results during deployment in the real world.<sup>[1a,14]</sup> The variety of flexible and stretchable sensors<sup>[15]</sup> and electronic or tactile skin<sup>[10d,16]</sup> can offer better solutions for integration of sensors on soft robotic structures. The sensors can provide instantaneous deformations (proprioception) or the real-time state of the soft robot's body.<sup>[1b]</sup> However, most of the reported sensors<sup>[15a,b]</sup> have limited conformability with soft objects or surfaces and are not readily customizable to suit the dimension, shape, and functionality of the soft robots. Further, the number of sensors that can be accommodated on the soft robotic surface is limited, thus hindering the desired

P. Karipoth, A. Christou, A. Pullanchiyodan, R. Dahiya  
Bendable Electronics and Sensing Technologies (BEST) Group  
James Watt School of Engineering  
University of Glasgow  
G12 8QQ, UK  
E-mail: Ravinder.Dahiya@glasgow.ac.uk

 The ORCID identification number(s) for the author(s) of this article can be found under <https://doi.org/10.1002/aisy.202100092>.

© 2021 The Authors. Advanced Intelligent Systems published by Wiley-VCH GmbH. This is an open access article under the terms of the Creative Commons Attribution License, which permits use, distribution and reproduction in any medium, provided the original work is properly cited.

DOI: 10.1002/aisy.202100092

performance of the soft robot.<sup>[17]</sup> The seamless integration of sensors and actuators throughout the body of a soft robot, just as biological organisms have, can help resolve such challenges.

Addressing the earlier need, herein, we present soft structures with intrinsic strain sensing provided through “seamlessly embedded” sensing material. The fully embedded sensing materials in the soft robotic structure provide intrinsic strain-sensing capability without occupying additional space. The custom-made graphite paste<sup>[1e]</sup>-based ultrastretchable (900%), highly sensitive ( $10^3$  up to  $\approx 200$  and of the order of  $10^5$  at around 700% linear strain), and fast-responding strain sensors (detailed fabrication given in Experimental Section) presented here can be easily embedded in the soft robotic structures. Tiny permanent magnets are incorporated at the ends of worm-like soft robotic structures to allow controlled movement.<sup>[18]</sup> The sensing and the potential for “proprioceptive soft robots”<sup>[1b]</sup> have been demonstrated through magnetically driven soft robots with a worm-like tubular body, as schematically shown in **Figure 1**. Specifically, soft robots with inchworm- (phylum: arthropods) (Figure 1a) and earthworm (phylum: annelids) (Figure 1c)-like shapes and movements have been developed. The graphite paste is fully

embedded in the soft robotic structures, following a bioinspired approach (Figure 1b) to provide instantaneous feedback about deformation. The presented solution can also be used with other soft robots that are controlled using alternative actuation techniques such as pneumatic, electroactive, dielectric, shape memory (SMA), etc.<sup>[19]</sup> The inchworm robot presented here utilizes the ultraflexibility of the developed strain sensor to track its locomotion resembling a real inchworm (Figure 1a,d). Likewise, the cyclic locomotion of earthworm-type soft robot utilizes the ultra-stretchability of the developed strain sensor for precise closed-loop feedback control (Figure 1c,d). These results demonstrate new possibilities for using soft robots with intrinsic sensing in applications such as delicate surgery inside the body.

## 2. Results and Discussion

### 2.1. Performance of the Ultrastretchable Strain Sensor

Ultrastretchability of sensors, in particular strain sensors, is crucial for soft robotic applications. In this context, we fabricated an ultrastretchable soft tubular strain sensor using the graphite

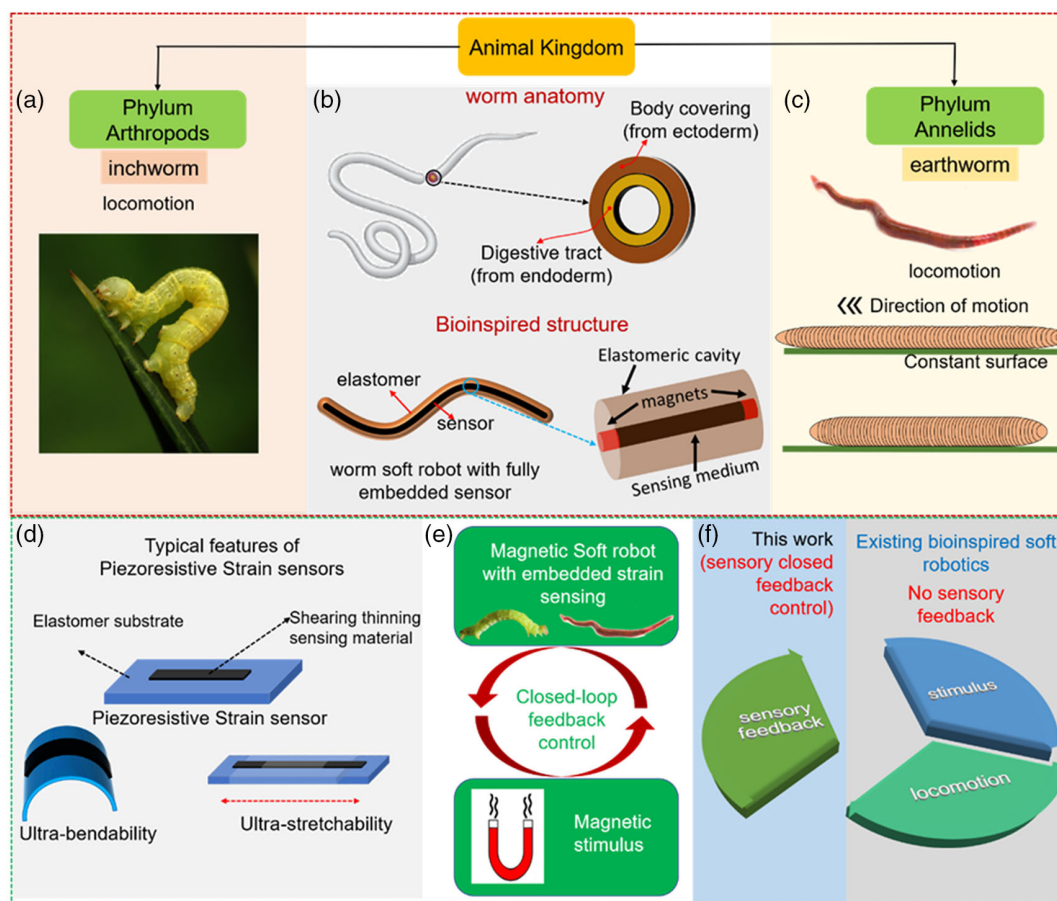


**Figure 1.** Concept of the bioinspired earthworm and inchworm soft robots with seamlessly embedded sensors. a) Locomotion of inchworm (Image: Katja Schulz/Flickr, reproduced under the terms of the CC-BY Creative Commons Attribution 4.0 International license (<https://creativecommons.org/licenses/by/4.0/>)). b) General anatomy of worm-like organisms and the design and cross-section view of the soft robot with embedded sensor. c) Locomotion of earthworm (Image: Brian Gratwicke/Flickr, reproduced under the terms of the CC-BY Creative Commons Attribution 4.0 International license (<https://creativecommons.org/licenses/by/4.0/>)). d) typical features of piezoresistive elastomeric strain sensors, e) theme of this work, and f) significance of this work with respect to state of art.

paste material and Ecoflex (fabrication and characterization procedure given in Experimental Section) and demonstrated its performance (see Movie S1, Supporting Information) for potential soft robotic applications. The outer diameter of the strain sensor is  $\approx 2$  mm. **Figure 2a** shows the images of the strain sensor with 0% and 200% stretching. The fabricated sensor was characterized for its electromechanical performance using a custom strain response arrangement with two stepper motors controlled by a custom LabView program. The two ends of the sensor are attached at the edge of each of the stepper motor platform and linearly strained by the synchronous backward and forward motion of the motors. The sensor's instantaneous resistance is recorded with a digital multimeter and the LabView interface. As shown in **Figure 2b**, the sensor exhibited significant and periodic variation of resistance with respect to the applied cyclic linear strain. As the strain increases, the resistance increases to a maximum value in proportion to the applied strain. For example, the maximum relative change of resistance,  $\Delta R/R_0$ , was around 13%, 30%, 100%, 150%, and 300% for maximum applied strain of 5%, 10%, 50%, 100%, and 200%, respectively. Finally, to find the maximum stretchable limit, the device was stretched, as shown in **Figure 2c**, until the elastomer snapped. As evident from the figure, the device was able to stretch up to 900% without damage. At this elongation, the device snapped at the contact end, where it experienced greater tension while stretching. The obtained stretchability is in accordance with the stretchable limits of Ecoflex of up to 900%.<sup>[20]</sup> The very high values ( $\approx 5$  k)

$\Delta R/R_0$  exhibited by the fabricated sensor are significantly higher than the strain sensors reported in the literature<sup>[21]</sup> (see **Figure S1**, Supporting Information) with similar materials and designs.<sup>[15a,22]</sup> The ultrastretchability of the strain sensor is demonstrated in the **Movie S2**, Supporting Information, and the corresponding sensor response is shown in **Figure 2d** (Here, the stretchability was up to  $\approx 800\%$  before it broke as device–device variation in the maximum breakpoint was expected.) As shown in **Figure 2d**, the sensor is highly sensitive, and the resistance increases slowly and reaches a maximum at the break point. This is attributed to the fact that with the stretching of the elastomeric sensor, the conducting graphitic particles move apart and reduce the percolation path and electrical conductivity. This is evident from the sensitivity of the order of  $10^3$  up to  $\approx 200$  and of the order of  $10^5$  at around 700%. The response variation is linear in the region 100–600%, as evident from the figure. The slight fluctuations in the response are because of the manual nonprogrammed stretching by hand. It may be noted that even though the stretchability of the order of 900% assures the safe deployment of these ultrastretchable sensors, the device will be more reliable in the operating ranges slightly below the stretchability limits. The sensitivity of the ultrastretchable design may be also dependent on various other factors such as conductive matrix, relative distribution of the particles, available electrical conduction (percolation) paths and thereby the degree of reconfiguration, the cross section perpendicular to the direction of stretching, etc.

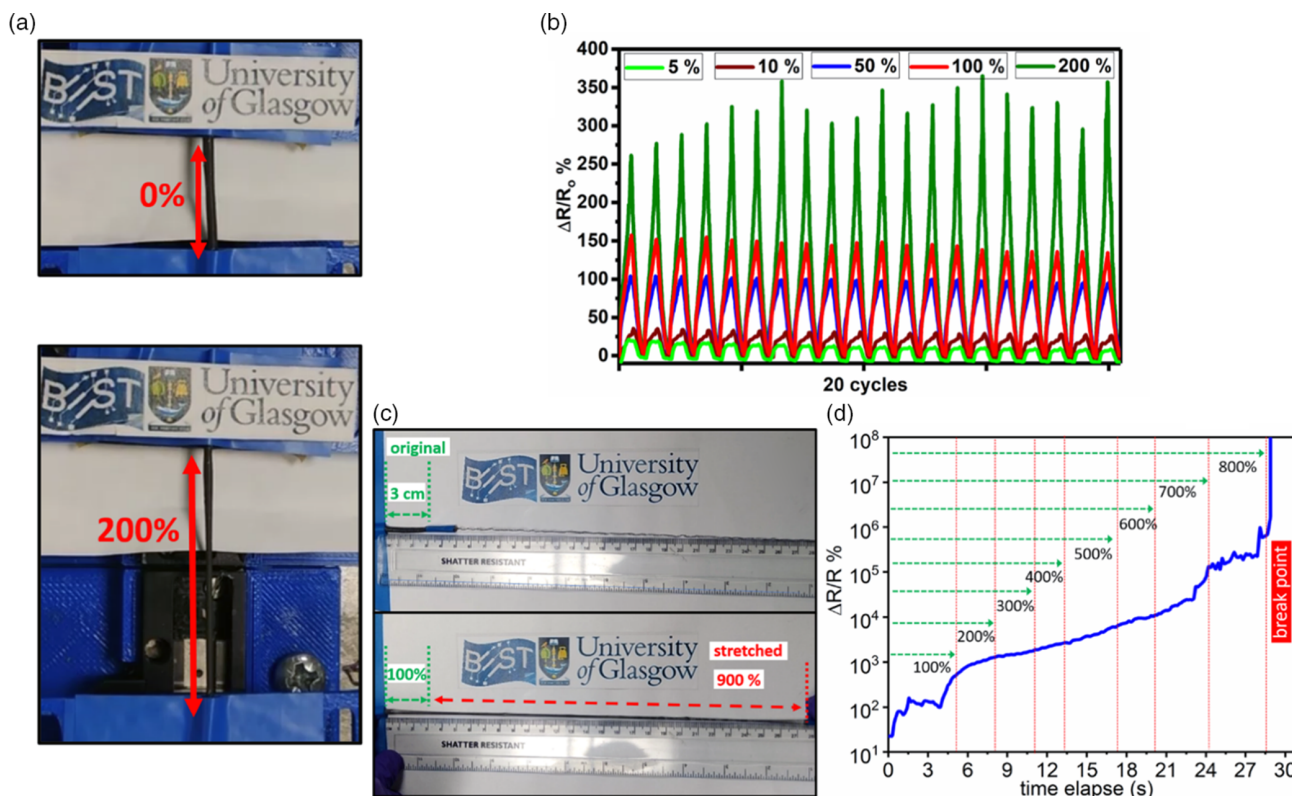


**Figure 2.** a,b) Controlled stretching of ultrastretchable tubular strain sensor for 0% (a) and 200% (b) dynamic strain response resistance variations of the strain sensor measured for 20 continuous cycles up to 5, 10, 50, 100, and 200% linear strain. c) Testing the break limit of the sensor (900%) and d) the image of electrical performance under 700% strain.

## 2.2. Application of the Fully Embedded Strain-Sensing System for Biomimetic Soft Robots

Bringing together the sensing capability of our developed ultra-stretchable strain sensor, flexibility of the elastomeric medium (Ecoflex), and established concepts of magnetically driven soft robots, we have designed the earthworm- and inchworm-type soft robots and demonstrated their external magnetic field-driven movements with intrinsic sensing and closed feedback control. The earthworm soft robot uses the stretchability and corresponding response of the strain sensor and for this purpose, the ultra-stretchable tubular design of the sensor was further improved (details given in Experimental Section) to fabricate the soft robot, which can be manipulated via external magnetic field. The fabricated earthworm robot is  $\approx 4.5$  cm in length and 4 mm in diameter, resembling an earthworm body (typically having diameter  $\approx 3$  mm and length of the order of few cm), which is boneless and can be elongated by 100–200% of its original length during locomotion. In the fabricated soft robot, the hollow cylindrical Ecoflex acts as the soft elastic tissue of the earthworm and the inner graphite paste channel as its sensing system. The two NdFeB magnet pairs embedded within soft body which can actuate forward or backward depending upon the direction of the applied external magnetic field act as the muscular system to

enable the locomotion of earthworm-type robot. The arrangement for the demonstration of the earthworm soft robot locomotion is shown in **Figure 3a**, as well as Supporting Information, Figure S2, Supporting Information. For this purpose, a transparent tube with a diameter of  $\approx 1.5$  cm is mounted horizontally and the tubular worm-like soft robot is placed in the middle of the tube along the axis. Two NdFeB permanent magnets ( $50 \times 50 \times 5$  mm, 24 kg vertical pull, from Magnet Expert Ltd. UK) were attached to the two linear motor stages and placed just below the tube close to the head and tail of the earthworm robot in such a way that they controlled the two ends of the soft robot (Figure 3a). Holding the tail stationary with the magnet (motor), the other linear motor moves forward (away from the first motor) and as a result the other end of the earthworm robot stretches. This is accompanied by simultaneous proportional increase in the strain and thereby increases the sensor output. The magnet (motor) moves forward and stretches the earthworm robot until the resistance value reaches the upper-threshold value of resistance (5 k $\Omega$ ), which can be set in the LabView program based on desired stretching in each step. The motor at the tail end is programmed to respond to the upper-threshold resistance value and it moves forward as soon as the threshold value is reached. The magnet attached to the motor thus drags the tail portion of soft robot forward so that it contracts to its original length. During this, the resistance also

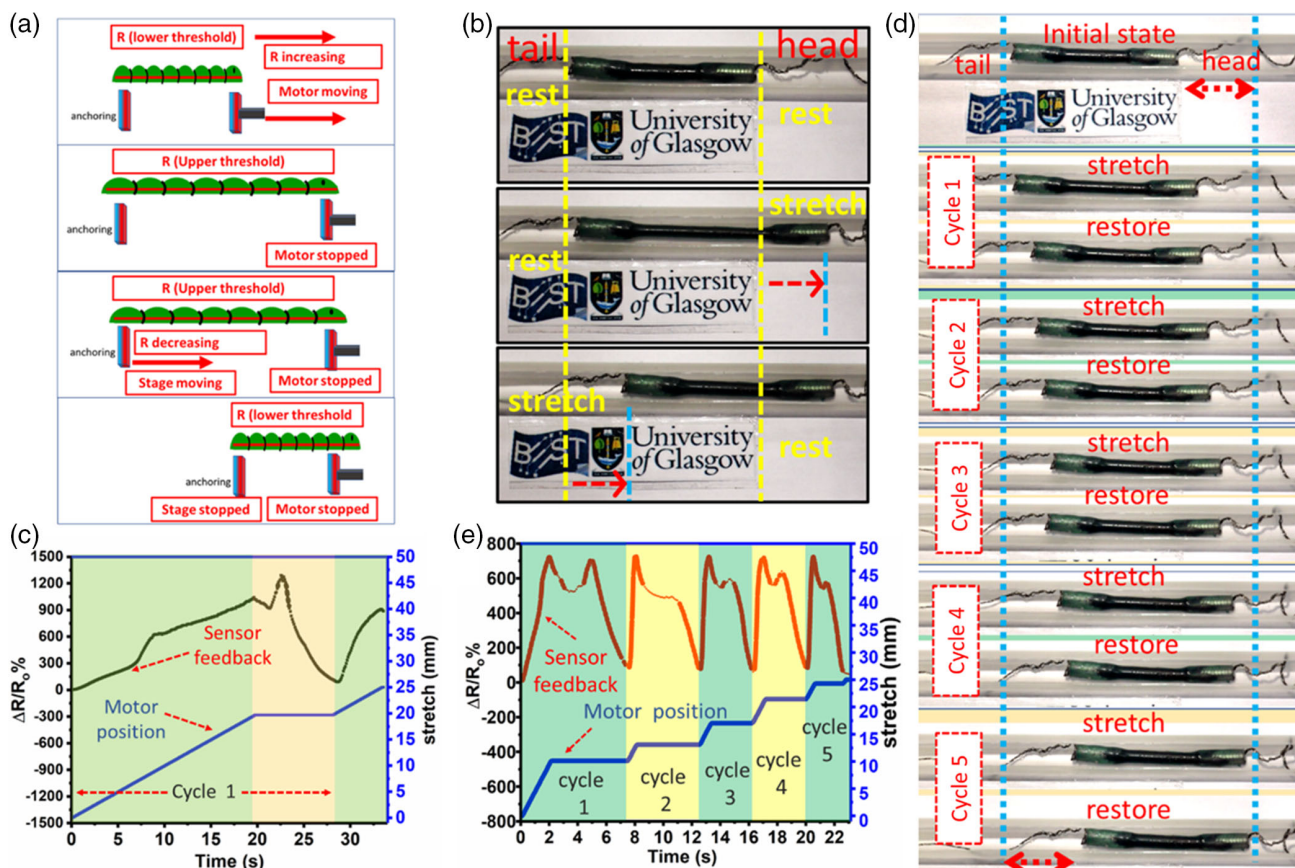


**Figure 3.** a) Concept and sequence of earthworm soft robot locomotion. b) Single-cycle closed-loop-controlled locomotion of earthworm robot and c) the corresponding sensor response and motor position. d) Consecutive five cycles of robotic actuation and e) corresponding sensor response and motor position.

decreases and once the resistance reaches the lower-threshold value (corresponding to equilibrium state), the motor at the head end of the soft robot moves, leading to further earthworm-type movement. In our experiment, even though both the motors can be made to modulate under closed feedback loop, for convenience, as well as to demonstrate the adaptiveness of the closed-loop soft robot actuation to unprogrammed stimulus, the rear motor is operated under manual control and front motor under automatic (closed loop) control. These cycles are repeated to obtain (See Supplementary Movie S3, Supplementary Information) controlled movement of soft robots, mimicking the earthworm locomotion, as shown in Figure 3a. Figure 3b shows one such actuation cycle of the soft robot and Figure 3c shows the corresponding strain sensor response and the instantaneous motor position being controlled by closed feedback. As the motor moves,

the resistance reaches an upper threshold of around 1150% or initial value where motor stops, and the earthworm robot was stretched up to around 33% of its original length. Once the soft robot is restored to its lower-threshold resistance ( $\approx 1$  k $\Omega$ ) state, the motor moves again. Here, the one cycle of distance 2.5 cm was completed in 33 s (average speed:  $\approx 0.8$  cm  $s^{-1}$ ). Figure 3d,e shows similar soft robotic locomotion for five consecutive cycles of smaller strokes traversing a total distance of 2.5 cm in 23 s (average speed:  $\approx 0.1$  cm  $s^{-1}$ ). Assuming the tube as a blood vessel or other internal organ of the body, one can guess the advances possible with such controlled movements in the biomedical field, for example, clearing the blockage in a blood vessel.

We also developed a new inchworm (Figure 4a)-type soft robot (fabrication procedure given in Experimental Section), which utilizes the bendability of the strain sensor. The cross section and

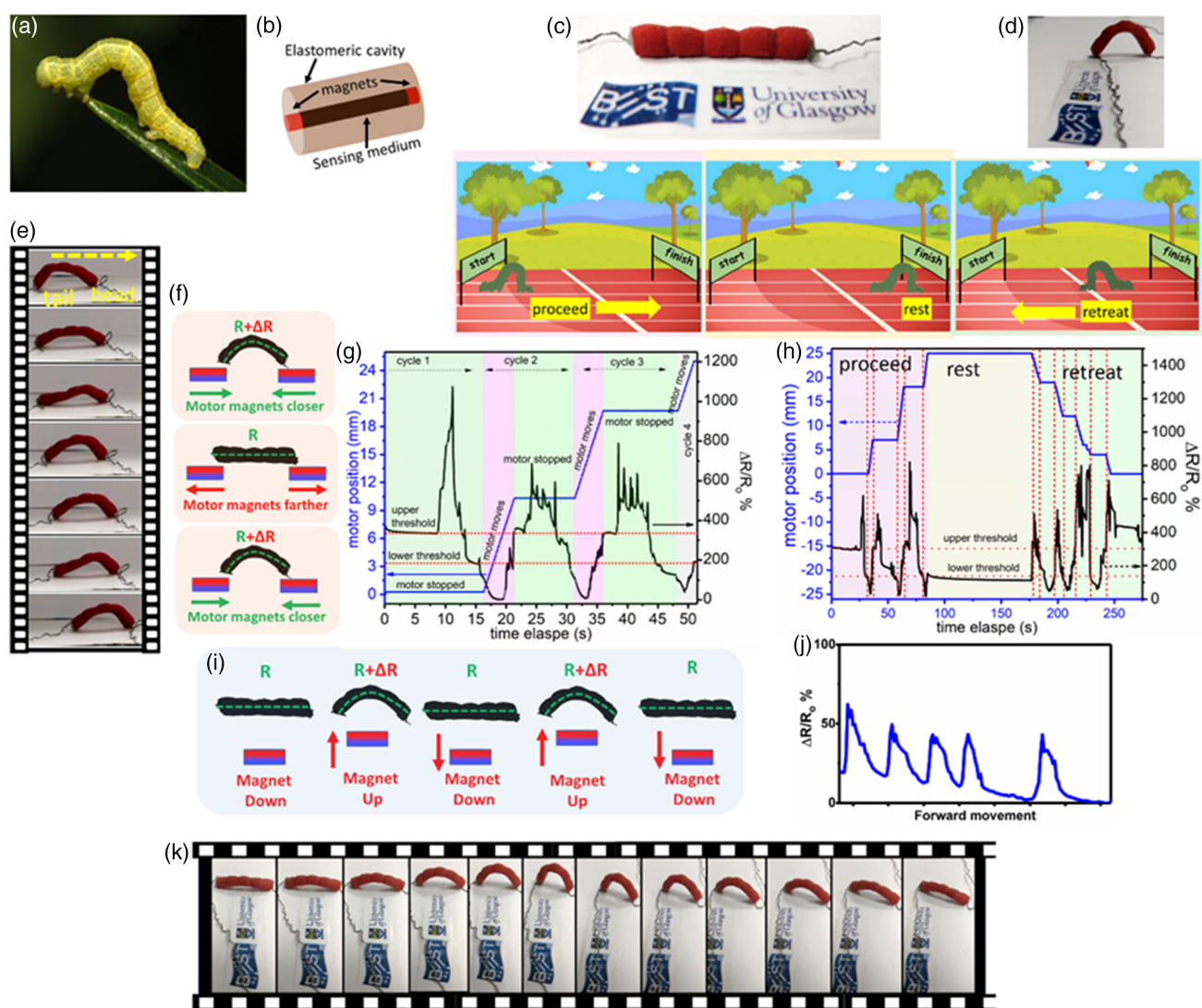


**Figure 4.** a) Inchworm (Image: Katja Schulz/Flickr, reproduced under the terms of the CC-BY Creative Commons Attribution 4.0 International license (<https://creativecommons.org/licenses/by/4.0/>)), b) cross-section view of inchworm-type soft robot. c) Fabricated inchworm soft robot, d) in bending configuration and e) movement and f) Locomotion mechanism with magnetic field movement. g) Instantaneous strain-sensing response during locomotion. h) locomotion with forward and reverse direction. i) Schematic of locomotion with single magnet actuation. j) Sensor response during single magnet actuation. k) Locomotion cycles with single magnet actuation.

image of the fabricated inchworm-inspired magnetic soft robot are shown in Figure 4b,c, respectively. The inchworm robot is around 4 cm in length and has cross-section area of around 6 mm. Here, Ecoflex acts as the soft elastic body of the inchworm and the inner graphite paste channel as its sensing system. The two NdFeB magnet pairs embedded within the soft body can actuate forward or backward motion depending upon the direction of the applied external magnetic field enabling the locomotion of the inchworm robot. When there is no external magnetic field, the soft robot lies in the flat position as in Figure 4c. Figure 4d shows the bending state of the inchworm robot. Figure 4e shows several cycles of the closed-feedback-controlled inchworm-inspired locomotion. The magnetic actuation scheme is schematically shown in Figure 4f and in Figure S2, Supporting Information. The actuation protocol is similar to the one followed for the earthworm soft robot locomotion discussed in the previous section and Figure 3a, except that the two linear motors (thereby attached magnets) move closer from the equilibrium position while they move apart for earthworm motion. This is in accordance with the fact that the earthworm motion relies on stretching deformation, whereas inchworm locomotion relies on bending deformation. Also, the demonstration is conducted in the open stage for unrestricted bending deformation as compared with the earthworm motion within a tube. In a typical experimental procedure, assuming the soft robot initially in the flat configuration, the two magnets attached to two linear motors are aligned in the head and tail regions of the soft robot. Now, the sensor resistance of the soft robot will be minimum. Maintaining the head firm with the magnet (motor), the other linear motor (tail region) is moved forward (toward the head motor) and as a result the inchworm robot bends, anchored at its head and tail. The bending deformation of the robot is proportional to the proximity of the two motors and is reflected by the corresponding systematic increase in sensor resistance. When the resistance reaches the upper threshold, the motor stops in response to the sensor feedback. The motor (head region) then moves forward, transforming the bend worm toward the flat state accompanied by the decrease in resistance. When the lower-threshold resistance is reached, the tail end motor again starts to move, approaching the head constituting the next cycle of locomotion. In our experiment, even though both the motors can be made to modulate under closed feedback loop, for convenience, as well as to demonstrate the adaptiveness on the closed-loop soft robot actuation to unprogrammed stimulus, the front motor is operated under manual control and back motor under automatic (closed-loop) control. These cycles are repeated to obtain (See Movie S4 in supplementary information) controlled movement of soft robots mimicking the inchworm locomotion, as shown in Figure 4a. Figure 4g shows the corresponding strain sensor response and the instantaneous motor position being controlled by closed feedback loop for three consecutive cycles. The lower- and upper-threshold resistances ( $\Delta R/R_0$ ) for feedback are around 200% and 350%, respectively.

The resistance variation during inchworm locomotion is much lower as compared with the earthworm locomotion as the former utilizes the stretchability and latter utilizes the bendability. The soft robot completes three cycles of locomotion with a total distance of 25 mm in around 50 s, which could be even faster if both

motors were controlled automatically. The few random spikes in the resistance are attributed to the frictional disturbance between the surface and the soft robot. However, for the smooth transition of the motor, unaffected by these noises, various other parameters such as tolerance, stabilization, etc. related to the motor driver and feedback program can be chosen. Figure 4h shows similar locomotion cycles with forward and reverse direction. Here, in the forward direction, the closed-loop locomotion is in the same manner as in Figure 4g. Once the soft robot reaches the target point and remains at rest (no stimulus), the motor also remains stationary. Once the motor is set in reverse movement mode and manually operated, the other motor can be driven under sensor feedback response of the soft robot, thus continuing the cyclic locomotion in the reverse direction. This demonstration also asserts the potential of the presented soft robot control approach for task-oriented path planning. Unlike earthworm locomotion, the presented magnetic inchworm soft robot could be manipulated by magnetic field by two schemes—the one by the already discussed two-magnet mode and the other is with a single-magnet mode. Here, when a magnet is brought toward and moved away from the middle region of the robot in a periodic fashion (schematically shown in Figure 4i), the soft robot exhibits systematic inchworm-inspired locomotion cycles, as shown in Figure 4k. The corresponding systematic variation of strain response is shown in Figure 4j. When the soft robot is in the bent state, the resistance is increased by 36%, as compared with its flat equilibrium state. It may be noted that the relative change in resistance as well as the noise is less as compared with the two-magnet locomotion scheme (Figure 4g). This is because the two magnets strongly anchor the soft robot on the moving surface and closely interact with the soft robot, yielding a more time-dependent dynamic strain. At the same time, in the latter case, the single magnet does not anchor the soft robot on the locomotion surface and therefore the dynamic stress during actuation is lesser. However, the two-magnet actuation provides better controlled locomotion than the single magnet in the presented scenario.

### 3. Conclusion

The soft robotic earthworm and inchworm locomotion experiments show that the instantaneous feedback from the fully embedded intrinsic strain sensors can provide the critical information needed to manipulate the soft robots. This will impart the precision and greater adaptability to soft robots to operate in diverse environments. The soft structures with seamlessly embedded sensors, as in biological organs, will transform soft robotics by enabling better control over the movements. This article demonstrated the first example of such sensory integration in a record stretchable (900%) soft structure. Using this strain-sensitive material, Ecoflex and NdFeB magnets, we fabricated biomimetic earthworm and inchworm soft robots with fully embedded strain sensors and demonstrated their controlled locomotion and simultaneous sensing capability. The demonstration of closed-loop-controlled bioinspired soft robot locomotion shows the potential of intrinsic-sensing stimulus-responsive soft robotics for real applications and brings soft robotics a step closer to biological systems.

## 4. Experimental Section

**Ultrastretchable Strain Sensor Fabrication:** The graphitic sensing material was prepared by mixing 2 wt% of dispersant Triton X-100 (Sigma Aldrich) and 5 wt% ethyl cellulose in terpineol (Sigma Aldrich) and magnetically stirred for 2 h. Following this, graphite powder was added and stirred continuously for 12 h. The hollow elastomer tubular body of the ultrastretchable soft robot was obtained by following the replica molding approach. A solid plastic rod of diameter of around 1 mm was utilized as a mandrel over which a thoroughly mixed Part A and Part B Ecoflex 00-30 was applied as a thin layer. Once the elastomer was cured, the plastic core was removed to obtain a hollow elastomer tube of desired length. Then, the synthesized graphite paste was carefully filled inside the tube with the help of a syringe. Afterward, electrical contacts were made at both ends of the elastomer and were encapsulated with silver paste. The fabricated tubular strain sensor was investigated for its mechanoresponse, using the same arrangement, as given in Supporting Information.

**Fabrication of Earthworm- and Inchworm-Based Biomimetic Locomotive Soft Robots:** For the fabrication of earthworm soft robot, the ultrastretchable tubular design of the strain sensor was further improved in such a way that it was manipulated via external magnetic field. A hollow tubular elastomeric structure was first obtained as explained previously, with a slightly larger diameter of 4 mm and length of 4.5 cm. After conducting a similar procedure, as in the case of the ultrastretchable strain sensor, the two ends (head and tail) of the tubular structure were made magnetically active by a set of ten numbers of tiny N42-grade (each of 3 mm dia., 1 mm thick, 0.19 kg vertical pull) NdFeB magnets (from Magnet Expert Ltd, UK) on both ends. Afterward, the electrical contacts were made from both sides.

The inchworm soft robot was fabricated using a similar approach, as in the case of earthworm soft robot, except that a 3D-printed mold was utilized. Ecoflex prepolymer mixture (with coloring additives) was poured in a 3D-printed mold of dimensions 4 cm length and 0.6 cm diameter, resembling an inchworm with an inner hollow channel of 1 mm diameter. Once the elastomer was cured, the inchworm-like elastomeric structure was removed from the mold and sensitive graphite paste was filled inside the tubular channel. Further, the ends of the elastomer were sealed with ten numbers of tiny N42-grade (each of 3 mm dia., 1 mm thick, 0.19 kg vertical pull) NdFeB magnets (from Magnet Expert Ltd, UK) on both ends. Afterward, the electrical contacts were made from both sides.

## Supporting Information

Supporting Information is available from the Wiley Online Library or from the author.

## Acknowledgements

This work was supported in part by the Engineering and Physical Sciences Research Council (EPSRC) through Engineering Fellowship for Growth (EP/R029644/1) and European Commission through Marie Skłodowska-Curie Actions International Fellowship (H2020-MSCA-IF-2017-798639).

## Conflict of Interest

The authors declare no conflict of interest.

## Data Availability Statement

Research data are not shared.

## Keywords

bioinspired systems, intrinsic sensing, sensory feedback, soft robots, strain sensors

Received: May 9, 2021

Revised: July 17, 2021

Published online: September 1, 2021

- [1] a) S. Kim, C. Laschi, B. Trimmer, *Trends Biotechnol.* **2013**, *31*, 287; b) H. Wang, M. Totaro, L. Beccai, *Adv. Sci.* **2018**, *5*, 1800541; c) U. G. Wegst, H. Bai, E. Saiz, A. P. Tomsia, R. O. Ritchie, *Nat. Mater.* **2015**, *14*, 23; d) R. S. Dahiya, M. Valle, in *Robotic Tactile Sensing: Technologies And System*, Springer Science & Business Media, New York **2013**; e) O. Ozioko, P. Karipoth, P. Escobedo, M. Ntagios, A. Pullanchiyodan, R. Dahiya, *Adv. Intell. Syst.* **2021**, <https://doi.org/10.1002/aisy.201900145>; f) R. Dahiya, N. Yogeswaran, F. Liu, L. Manjakkal, E. Burdet, V. Hayward, H. Jörntell, *Proc. IEEE* **2019**, *107*, 2016; g) Y. Kim, H. Yuk, R. Zhao, S. A. Chester, X. Zhao, *Nature* **2018**, *558*, 274.
- [2] S. Niu, Y. Luo, Y. Shen, K. J. Kim, in *2015 IEEE Int. Conf. on Robotics and Biomimetics (ROBIO)* IEEE, Piscataway, NJ, USA **2015**, pp. 499–504; <https://doi.org/10.1109/ROBIO.2015.7418817>.
- [3] W. Wang, J.-Y. Lee, H. Rodrigue, S.-H. Song, W.-S. Chu, S.-H. Ahn, *Bioinspir. Biomim.* **2014**, *9*, 046006.
- [4] D. E. Koditschek, R. J. Full, M. Buehler, *Arthropod. Struct. Dev.* **2004**, *33*, 251.
- [5] W. Kristan, in *The Oxford Handbook Of Invertebrate Neurobiology*, Oxford University Press, Oxford, UK **2019**, p. 451.
- [6] a) T. G. Thuruthel, B. Shih, C. Laschi, M. T. Tolley, *Sci. Rob.* **2019**, *4*, eaav1488; b) G. M. Whitesides, *Angew. chem., Int. Ed.* **2018**, *57*, 4258; c) C. Laschi, B. Mazzolai, M. Cianchetti, *Sci. Rob.* **2016**, *1*, eaah3690; d) S. Coyle, C. Majidi, P. LeDuc, K. J. Hsia, *Extreme Mech. Lett.* **2018**, *22*, 51; e) H. Zhao, R. Hu, P. Li, A. Gao, X. Sun, X. Zhang, X. Qi, Q. Fan, Y. Liu, X. Liu, M. Tian, G. Tao, L. Qu, *Nano Energy* **2020**, *76*, 104926; f) T. Jin, Z. Sun, L. Li, Q. Zhang, M. Zhu, Z. Zhang, G. Yuan, T. Chen, Y. Tian, X. Hou, C. Lee, *Nat. Mater.* **2020**, *11*, 5381.
- [7] a) J. Z. Ge, A. A. Caldern, N. O. Pérez-Arancibia, in *2017 IEEE Int. Conf. on Robotics and Biomimetics (ROBIO)*, IEEE, Piscataway, NJ, USA **2017**, pp. 834–841, <https://doi.org/10.1109/ROBIO.2017.8324521>; b) H. Fang, Y. Zhang, K. Wang, *Bioinspir. Biomim.* **2017**, *12*, 065003; c) H. Guo, J. Zhang, T. Wang, Y. Li, J. Hong, Y. Li, in *2017 IEEE Int. Conf. on Robotics and Automation (ICRA)*, IEEE, Piscataway, NJ, USA **2017**, pp. 4154–4159; <https://doi.org/10.1109/ICRA.2017.7989477>; d) J. Ning, C. Ti, Y. Liu, *J. Robot. Automat.* **2017**, *1*, 54.
- [8] a) N. W. Bartlett, M. T. Tolley, J. T. Overvelde, J. C. Weaver, B. Mosadegh, K. Bertoldi, G. M. Whitesides, R. J. Wood, *Science* **2015**, *349*, 161; b) E. W. Hawkes, L. H. Blumenschein, J. D. Greer, A. M. Okamura, *Sci. Robot* **2017**, *2*, eaan3028.
- [9] a) E. Dolph, C. Krause, D. Oleynikov, in *Robotic-Assisted Minimally Invasive Surgery*, Springer, New York **2019**, p. 329; b) C. Wang, Y. Sun, J. Xu, X. Liu, X. Zhou, X. Chen, in *2019 IEEE 4th Int. Conf. on Advanced Robotics and Mechatronics (ICARM)*, IEEE, Piscataway, NJ, USA **2019**, pp. 426–431, <https://doi.org/10.1109/ICARM.2019.8834213>; c) A. Stolt, M. Linderoth, A. Robertsson, R. Johansson, in *2012 IEEE Int. Conf. on Robotics and Automation*, IEEE, Piscataway, NJ, USA **2012**, pp. 1538–1543; <https://doi.org/10.1109/ICRA.2012.6224837>; d) O. Ozioko, P. Karipoth, M. Hersh, R. Dahiya, *IEEE Trans. Neural Syst. Rehabil. Eng.*, **2020**, *28*, 1344; e) O. Ozioko, R. Dahiya, *Adv. Intell. Syst.* <https://doi.org/10.1002/aisy.202100091>.

- [10] a) R. Pfeifer, M. Lungarella, F. Iida, *Commun. ACM* **2012**, *55*, 76; b) B. Trimmer, *Soft Rob.* **2014**, *1*, 231; c) O. Ozioko, W. Navaraj, M. Hersh, R. Dahiya, *Sensors* **2020**, *20*, 4780; d) P. Escobedo, M. Ntagios, D. Shakhivell, W. T. Navaraj, R. Dahiya, *IEEE Trans. Robot.* **37**, 683, **2021**; e) R. Mukherjee, P. Ganguly, R. Dahiya, *Adv. Intell. Syst.* **2021**, 2100036.
- [11] a) Y. Zhao, G. Meng, W. Zhang, *Smart Mater Struct.* **2020**, *29*, 055019; b) D. Ahmad, S. K. Sahu, K. Patra, *Polym. Test* **2019**, *79*, 106038; c) Z. Liao, M. Hossain, X. Yao, R. Navaratne, G. Chagnon, *Polym. Test* **2020**, 106478.
- [12] a) M. Calisti, G. Picardi, C. Laschi, *J. R. Soc. Interfaces* **2017**, *14*, 20170101; b) T. Umedachi, V. Vikas, B. A. Trimmer, in *2013 IEEE/RSJ Int. Conf. on Intelligent Robots and Systems*, IEEE, Piscataway, NJ, USA **2013**, pp. 4590–4595; <https://doi.org/10.1109/IROS.2013.6697016>.
- [13] D. Bruder, C. D. Remy, R. Vasudevan, in *2019 Int. Conf. on Robotics and Automation (ICRA)*, IEEE, Piscataway, NJ, USA, **2019**, pp. 6244–6250, <https://doi.org/10.1109/ICRA.2019.8793766>.
- [14] B. A. Trimmer, H.-T. Lin, A. Baryshyan, G. G. Leisk, D. L. Kaplan, in *2012 4th IEEE RAS & EMBS Int. Conf. on Biomedical Robotics and Biomechatronics (BioRob)*, IEEE, Piscataway, NJ, USA **2012**, pp. 599–605, <https://doi.org/10.1109/BioRob.2012.6290698>.
- [15] a) L. Duan, D. R. D'hooge, L. Cardon, *Prog. Mater. Sci* **2019**, 100617; b) M. Amjadi, K. U. Kyung, I. Park, M. Sitti, *Adv. Funct. Mater* **2016**, *26*, 1678; c) S. Cheng, Y. S. Narang, C. Yang, Z. Suo, R. D. Howe, *Adv. Mater. Interfaces* **2019**, *6*, 1900985; d) B. S. Homberg, R. K. Katzschmann, M. R. Dogar, D. Rus, *Auton. Rob.* **2019**, *43*, 681; e) Y. Lu, M. C. Biswas, Z. Guo, J.-W. Jeon, E. K. Wujcik, *Biosens. Bioelectron* **2019**, *123*, 167; f) Y. Kumaresan, H. Kim, Y. Pak, P. K. Poola, R. Lee, N. Lim, H. C. Ko, G. Y. Jung, R. Dahiya, *Adv. Electron. Mater.* **2020**, *6*, 2000058; g) M. Bhattacharjee, M. Soni, P. Escobedo, R. Dahiya, *Adv. Electron. Mater.* **2020**, *6*, 2000445; h) M. Bhattacharjee, P. Escobedo, F. Nikbakhtnasrabadi, R. Dahiya, *IEEE Internet Things J.*, **2021**, *8*, 5093-5100; i) W. Dang, V. Vinciguerra, L. Lorenzelli, R. Dahiya, *Flex. Print. Electron.* **2017**, *2*, 013003.
- [16] a) R. Dahiya, D. Akinwande, J. S. Chang, *Proc. IEEE* **2019**, *107*, 2011; b) C. G. Núñez, L. Manjakkal, R. Dahiya, *NPJ Flex. Electron.* **2019**, *3*, 1; c) M. Soni, R. Dahiya, *Philos. Trans. Roy. Soc. A*, **2020**, 378, 20190156.
- [17] a) C. F. Mateus, C. L. Barbosa, in *2007 SBMO/IEEE MTT-S Int. Microwave and Optoelectronics Conf.*, IEEE, **2007**, pp. 496–498, <https://doi.org/10.1109/IMOC.2007.4404313>; b) S. Kim, J. Kwon, S. Kim, B. Lee, *IEEE Photonics Technol. Lett.* **2000**, *12*, 678.
- [18] a) M. Li, N. A. Ostrovsky-Snyder, M. Sitti, F. G. Omenetto, *MRS Adv.* **2019**, *4*, 2787; b) E. B. Joyee, Y. Pan, *Soft Robot* **2019**, *6*, 333; c) M. Sitti, *Nat. Rev. Mater.* **2018**, *3*, 74.
- [19] H. Koshima, in *Mechanically Responsive Materials For Soft Robotics*, John Wiley & Sons, Hoboken, NJ, USA **2019**.
- [20] S. Ryu, P. Lee, J. B. Chou, R. Xu, R. Zhao, A. J. Hart, S.-G. Kim, *ACS Nano* **2015**, *9*, 5929.
- [21] a) C.-G. Zhou, W.-J. Sun, L.-C. Jia, L. Xu, K. Dai, D.-X. Yan, Z.-M. Li, *ACS Appl. Mater. Interfaces* **2019**, *11*, 37094; b) S. J. Park, J. Kim, M. Chu, M. Khine, *Adv. Mater. Technol.* **2016**, *1*, 1600053; c) Y. Wei, S. Chen, X. Yuan, P. Wang, L. Liu, *Adv. Funct. Mater.* **2016**, *26*, 5078; d) H. Hu, Z. Zhao, W. Wan, Y. Gogotsi, J. Qiu, *ACS Appl. Mater. Interfaces* **2014**, *6*, 3242; e) X. Wu, Y. Han, X. Zhang, Z. Zhou, C. Lu, *Adv. Funct. Mater.* **2016**, *26*, 6246; f) J. D. Pegan, J. Zhang, M. Chu, T. Nguyen, S.-J. Park, A. Paul, J. Kim, M. Bachman, M. Khine, *Nanoscale* **2016**, *8*, 17295; g) D. Kang, P. V. Pikhitsa, Y. W. Choi, C. Lee, S. S. Shin, L. Piao, B. Park, K.-Y. Suh, T.-I. Kim, M. Choi, *Nature* **2014**, *516*, 222; h) G. Shi, Z. Zhao, J. H. Pai, I. Lee, L. Zhang, C. Stevenson, K. Ishara, R. Zhang, H. Zhu, J. Ma, *Adv. Funct. Mater.* **2016**, *26*, 7614; i) S. Duan, Z. Wang, L. Zhang, J. Liu, C. Li, *Adv. Mater. Technol.* **2018**, *3*, 1800020; j) B. Park, J. Kim, D. Kang, C. Jeong, K. S. Kim, J. U. Kim, P. J. Yoo, T. I. Kim, *Adv. Mater.* **2016**, *28*, 8130; k) W. Lin, C. He, H. Huang, W. Zhao, Y. Qiu, X. Guan, Q. Zhang, Z. Wang, Z. Peng, *Adv. Mater. Technol.* **2020**, *5*, 2000008; l) J. Ye, T. Yang, Y. Zhang, L. Lin, *Adv. Mater. Interfaces* **2018**, *5*, 1800616; m) X. Liao, Z. Zhang, Z. Kang, F. Gao, Q. Liao, Y. Zhang, *Mater. Horiz.* **2017**, *4*, 502; n) Y. Zheng, Q. Jin, W. Chen, Y. Sun, Z. Wang, *J. Mater. Chem. C* **2019**, *7*, 8423.
- [22] X. Huang, Z. Yin, H. Wu, *Adv. Intell. Syst.* **3**, 2000194.